MANCHESTER
1824
The University of Manchester

Thesis Title

A thesis submitted to the University of Manchester for the degree of
Doctor of Philosophy
in the Faculty of Science and Engineering

2022

Damian Crosby
Department of Mechanical, Aerospace and Civil Engineering

Contents

Word Count: X

List of figures

List of tables

List of publications

Publications go here.

List of abbreviations

AUJ Actuated Universal Joint

2D Two Dimensional

3D Three Dimensional

COM Centre of Mass

DLS Damped Least Squares

DOF Degree(s) of Freedom

PID Proportional Integral Derivative

SHTP Sensor Hub Transport Protocol

MSB Most Significant Bit

LSB Least Significant Bit

I^2C Inter-Integrated Circuit

SPI Serial Peripheral Interface

UART Universal Asynchronous Receiver-Transmitter

DIO Digital Input/Output

IMU Inertial Measurement Unit

GOOP Graphical Object Oriented Programming

CS Chip Select

DFT Discrete Fourier Transform

Abstract

This is abstract text.

Declaration of originality

I hereby confirm that no portion of the work referred to in the thesis has been submitted in support of an application for another degree or qualification of this or any other university or other institute of learning.

Copyright statement

i The author of this thesis (including any appendices and/or schedules to this thesis) owns certain copyright or related rights in it (the "Copyright") and s/he has given The University of Manchester certain rights to use such Copyright, including for administrative purposes.

ii Copies of this thesis, either in full or in extracts and whether in hard or electronic copy, may be made *only* in accordance with the Copyright, Designs and Patents Act 1988 (as amended) and regulations issued under it or, where appropriate, in accordance with licensing agreements which the University has from time to time. This page must form part of any such copies made.

iii The ownership of certain Copyright, patents, designs, trademarks and other intellectual property (the "Intellectual Property") and any reproductions of copyright works in the thesis, for example graphs and tables ("Reproductions"), which may be described in this thesis, may not be owned by the author and may be owned by third parties. Such Intellectual Property and Reproductions cannot and must not be made available for use without the prior written permission of the owner(s) of the relevant Intellectual Property and/or Reproductions.

iv Further information on the conditions under which disclosure, publication and commercialisation of this thesis, the Copyright and any Intellectual Property and/or Reproductions described in it may take place is available in the University IP Policy (see `http://documents.manchester.ac.uk/DocuInfo.aspx?DocID=24420`), in any relevant Thesis restriction declarations deposited in the University Library, The University Library's regulations (see `http://www.library.manchester.ac.uk/about/regulations/`) and in The University's policy on Presentation of Theses.

Acknowledgements

Acknowledgements go here.

Chapter 1

A Literature Review of Terrestrial Robots with Robotic Tails and Their Functions

1.1 Introduction

The field of terrestrial robots with robotic tails is incredibly diverse, reflecting the many functions of tails in the animal kingdom. Even discounting tails used for fluid dynamics (swimming and flying robots), and focusing only on robots that use their tail during "terrestrial" locomotion (broadly defined as when a robot is moving along a contiguous surface, or jumping from one surface to another surface), there are many applications of robotic tails. In order to make sense of the state of the field, an abstract categorisation system is considered based on the environment the robot is in when the tail is active, the specific action the robot is taking to move itself in space, and what the specific function of the tail is with respect to the robot dynamics. Using this categorisation system, various examples are explored from a set of research articles selected using specific keywords. From this, conclusions can be derived about the general design and operation of robotic tails, which can be used to influence and guide the research covered in chapters **??**.

1.2 Research Methodology

Using three online publication repositories, *IEEE Xplore*, *Scopus* and *Web of Science*, a search query was conducted to find relevant publications. The query was tailored to include all publications with **tail*** or **appendage** in the title along with **robot*** (* indicates a wildcard suffix), but to exclude publications that concerned swimming, water walking, or flying robots, as using a tail as a rudder to influence fluid dynamics was outside of the scope of the research. Further exclusions were added upon experimentation with the query in order to remove false positives in areas such as chemistry (as molecules are often described as having "tails") or medicine (as it did not pertain to mobile robots and usually concerned biological structures such as proteins and cells). The date range was set from January 1980 to December 2018 to exclude outdated publications. The exact queries for each repository can

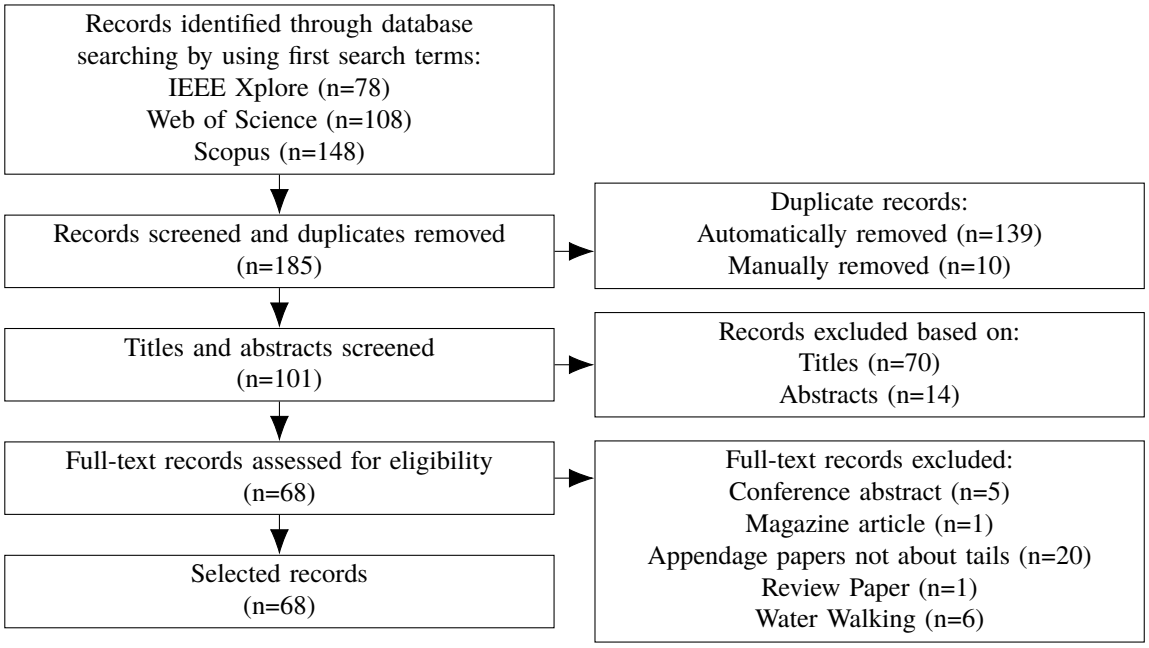

Figure 1.1: Flowchart of the publication selection process.

be found in table **??**.

As a result XX publications were discovered. After duplicates were removed and after screening abstracts and full texts, a total of XX unique publications were selected for inclusion. A flowchart of this process can be found in figure **??**.

1.3 Tail Functions of Terrestrial Robots

1.3.1 Categorisation System

The resulting publications represented a wide array of different robot designs and multiple forms of locomotion. Therefore, a simple categorisation system was required in order to better understand the majority of the functions of these tails. After careful analysis of the literature, two questions could be asked that provided common answers:

1. Is the robot on the ground, in the air or transitioning between those states when the tail is active?
2. What precisely is the robot doing when the tail is active?
3. What does the tail do to the dynamics of the robot (i.e. what would happen if there *wasn't* a tail present)?

Each question can then assign a tiered category to a publication based on the answer, the three tiers named *Environment*, *Action* and *Function*.

1. **Environment:** The general domain the robotic system is operating in when the tail is active. From the reviewed literature, three categories have been created:

- *Terrestrial:* A robot with an active tail when the robot is touching a surface, such as a robot driving along the ground.
- *Aerial:* A robot with an active tail when the robot is in free space, such as a robot which *has jumped* into the air, or is falling off a ledge.
- *Transition:* A robot with an active tail when the robot is just about to transition from between the two previous environments, such as a robot *just about* to jump into the air.

2. **Action:** The specific action the robot is performing when the tail is active. Most actions are unique to each environment, except for *hopping*.
   - *Straight:* A robot travelling across a surface maintaining its direction of travel.
   - *Accelerating:* A robot changing its velocity in the direction of travel across a surface. In the literature, this was a robot coming to complete stop, and starting from stationary.
   - *Turning:* A robot changing its direction of travel across a surface, such as a robot turning a corner.
   - *Balancing:* A robot undergoing external disturbances while travelling across a surface, typically due to adverse terrain, such as a robot navigating a rough and uneven surface without falling over.
   - *Hopping:* A robot executing a sequence of periodic jumps in order to travel across a surface, similar to the method of locomotion of a Kangaroo.
   - *Jumping:* A robot executing isolated non-periodic jumps, typically to transition from one surface to another at a different altitude and/or orientation.
   - *Falling:* A robot transitioning from one surface to another at a different altitude via the influence of gravity.
3. **Function:** The purpose of the tail when the robot is performing the action. These categories usually apply to multiple actions.
   - *Stability:* The tail is used to *maintain* some aspect of the robot's position and/or orientation from the start of the action.
   - *Initiation:* The tail is used to *change* some aspect of the robot's position and/or orientation from the start of the action.
   - *Amplification:* The tail is used to *amplify* the effects of an action by other parts of the robot (such as the legs) which changes the position and/or orientation.

For example, a robot with a tail that helps it increase it's apex when hopping, is in the *Transition* environment as it is about to transition from being on the ground to in the air when

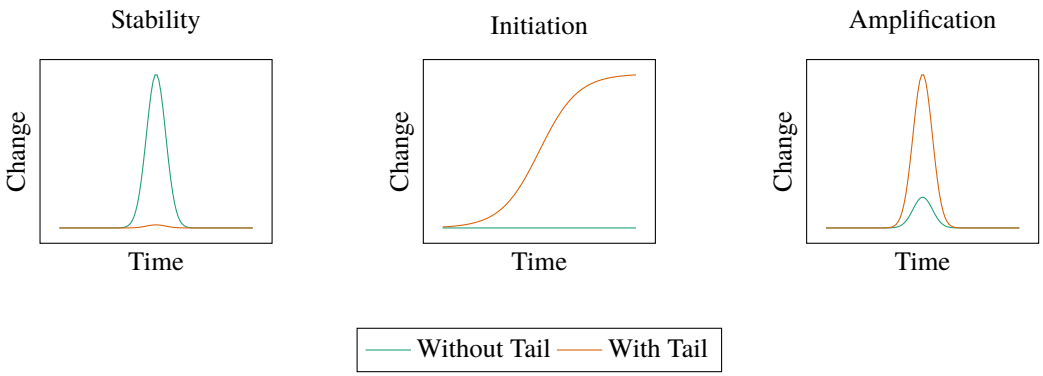

Figure 1.2: Abstract graphs of the different functions of the tail, with the magnitude representing some kind of change in the robot's position and/or orientation.

the tail is active. The robot itself locomotes by hopping, so it is performing a *Hopping* action, and since without the tail the robot would still be capable of hopping, but would not have such a tall apex, the tail can be considered to be performing *Amplification* of the robot's existing capabilities. Overall, this results in the categorisation *Transition* $\rightarrow$ *Hopping* $\rightarrow$ *Amplification*.

Another example is a robot with a tail that prevents it from falling over on rough terrain. The robot is in the *Terrestrial* environment as it is on the ground when the tail is active. The robot itself is performing a *Balancing* action as it is trying to remain upright during locomotion, and since without the tail the robot would fall over, the tail can be considered to be maintaining the *Stability* of the robot. Overall, this results in the categorisation *Terrestrial* $\rightarrow$ *Balancing* $\rightarrow$ *Stability*.

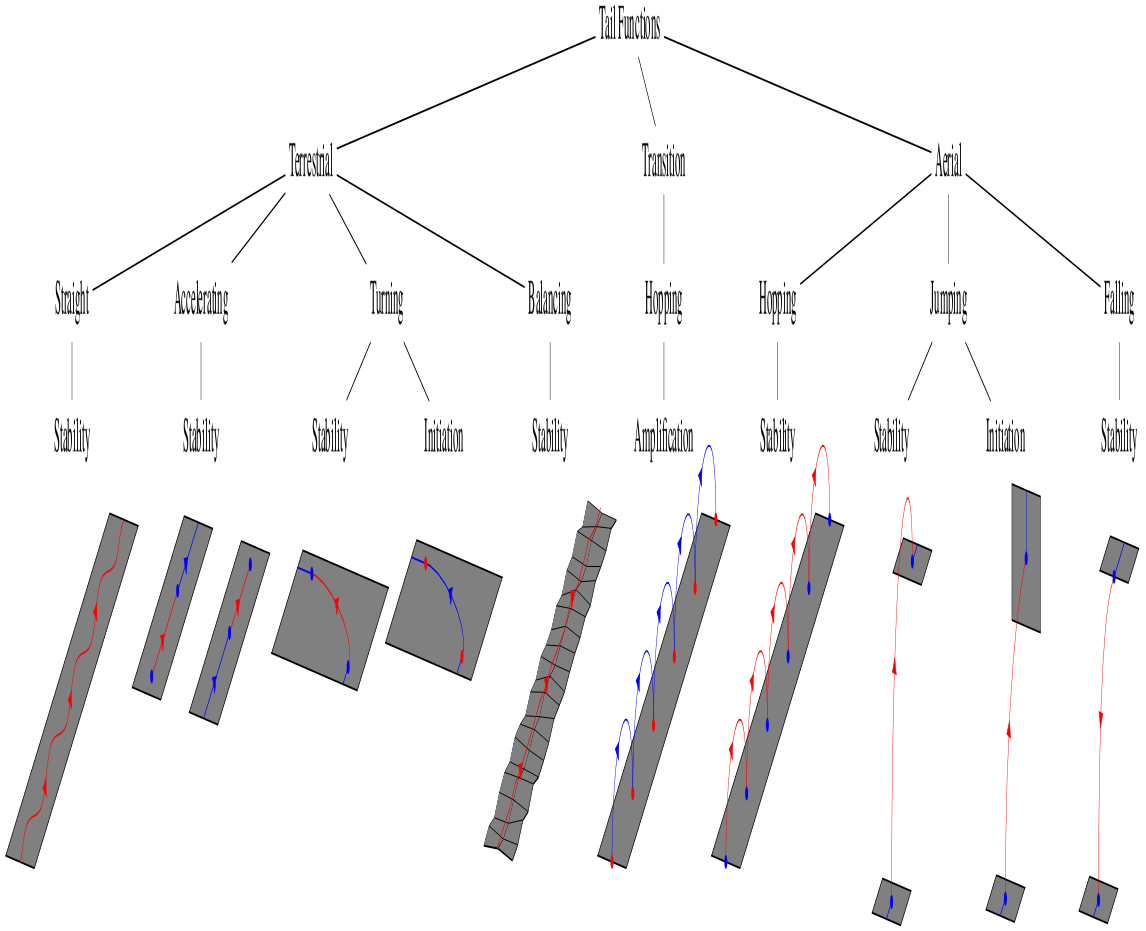

Figure 1.3: Tree diagram of all the categorisations found in the publications with accompanying visual diagrams.

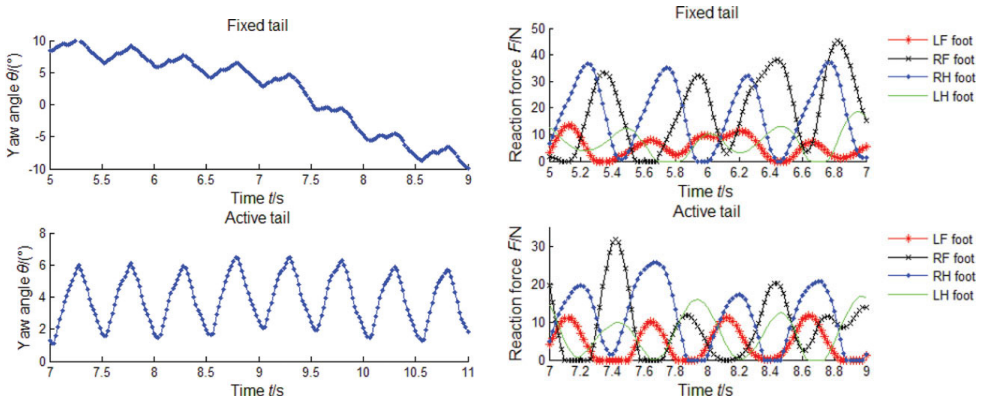

Figure 1.4: Data from **zhang2016effects** showing the effects of a static and dynamic tail on maintaining robot heading in a trotting gait.

1.3.2 Examples from each Category

1.3.3 *Terrestrial* → *Straight* → *Stability*

zhang2016effects uses a quadrupedal robot (Dcat), with a gait controlled by a **CPG!** (**CPG!**), an open loop control concept based on neural networks found in the spinal chords of vertebrates and invertebrate thoracic ganglia **ijspeert2008central**. A **CPG!** in robotics is typically constructed from a network of oscillators represented by a system of **ODE!** (**ODE!**), which accepts the input of another oscillator as a parameter in the system. By chaining these together, complex synchronised trajectories can be generated for multiple actuators in robot locomotion.

Upon initial experiments with a trotting locomotion with no active tail, the robot wouldn't maintain a set heading, it would slowly begin to drift in a circle. Visual observations noted that the robot would topple onto its front left leg that was in "swing" phase (lifted off the ground), and it would drag on the ground until in "stance" phase. This resulted in a difference between the **GRF!** (**GRF!**) of the left and right feet which caused the drift in locomotion path.

By implementing a swinging 1 **DOF!** (**DOF!**) tail that imparted an opposing torque to the direction of the topple, the differences between the left and right **GRF!** were reduced, and the robot could maintain its heading, as can be seen in figure **??**.

1.3.4 *Terrestrial* → *Accelerating* → *Stability*

patel2014rapid used inspiration from the Cheetah (*Acinonyx jubatus*) to improve the acceleration and braking capabilities of a wheeled robot (Dima). The research is based on findings from **williams2009pitch**, which shows that quadruped acceleration and deceleration in the animal kingdom is limited by their ability to constrain body pitch to prevent toppling over. It can be considered analogous to a motorcycle: accelerate too fast and the vehicle will "pop a wheelie" and potentially flip backwards, decelerate too fast and the opposite may occur.

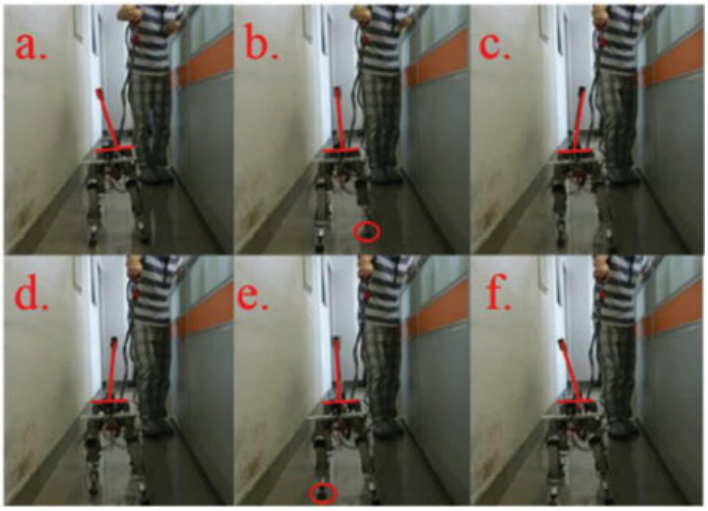

Figure 1.5: Image from **zhang2016effects** showing how the tail moves during the gait in order to correct for heading drift.

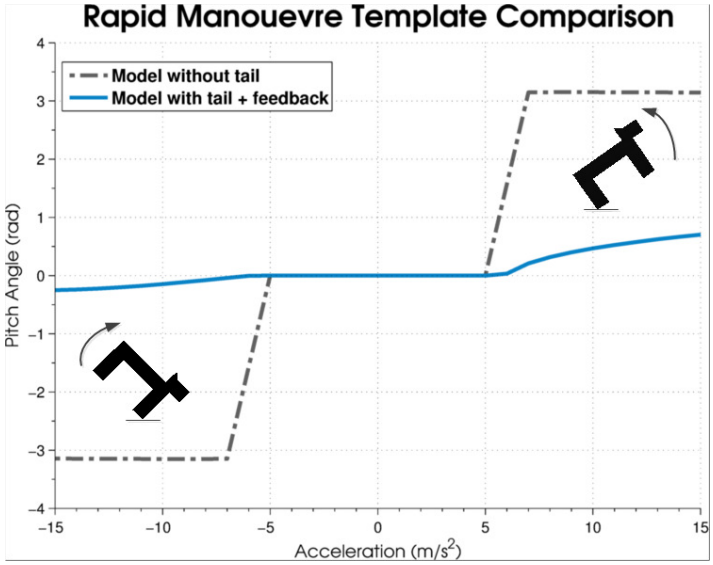

Figure 1.6: Simulation Data from **patel2014rapid** showing the how the body pitch would be reduced when accelerating of braking with an active tail.

Using a combined state feedback and **PI!** (**PI!**) controller based on the angular position of the tail, and the angular velocity of the tail and body, the researchers were able to increase the acceleration and braking capabilities of the robot by using the tail to generate an opposing torque to the direction of body pitch, as can be seen in figure **??**. This was verified by running a series of experiments, increasing the acceleration/braking magnitude until the robot failed to complete the test by toppling over.

Figure 1.7: Images from **patel2014rapid** showing the robot performing a rapid acceleration test with the tail.

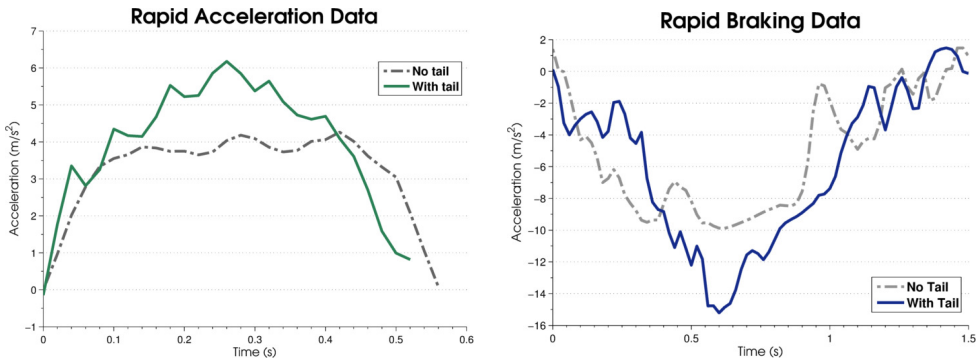

Figure 1.8: Experimental Data from **patel2014rapid** showing the maximum acceleration achieved with and without an active tail.

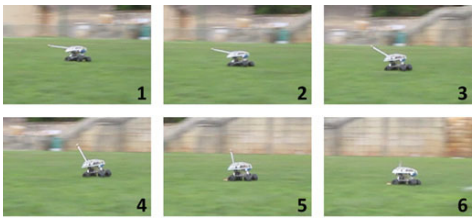

Figure 1.9: Images from **patel2015conical** showing the robot performing a turn with the tail.

1.3.5 *Terrestrial* → *Turning* → *Stability*

patel2013rapid, **patel2015conical** took similar inspiration from the Cheetah to allow for tighter turns by allowing greater lateral acceleration. **patel2013rapid** swings the tail out in a single motion in the direction of the turn, producing an opposing torque to the centrifugal force that would otherwise topple the robot during the turn. In contrast, **patel2015conical** moves the tail constantly in a conical motion, the direction of rotation in the direction of the turn. This also produces an opposing torque in the same fashion, but was not limited in duration, as in the first strategy the tail would eventually contact the ground. This allowed for turns of longer duration to be stabilised.

The control system and experimental procedures were similar to those in **patel2014rapid**.

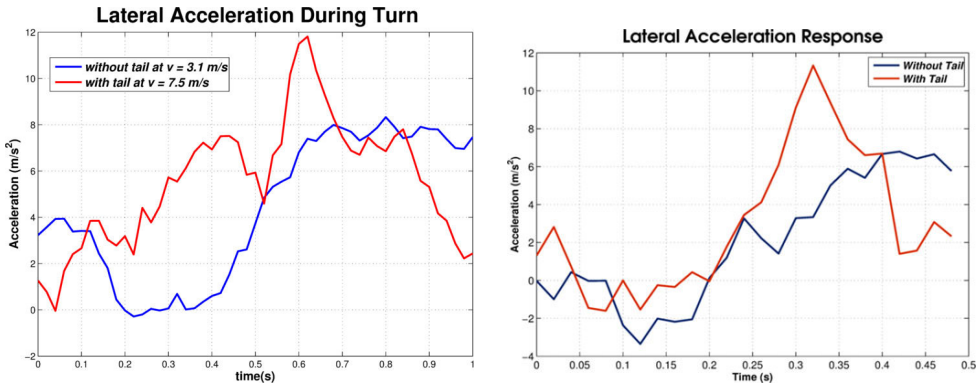

Figure 1.10: Experimental Data from **patel2013rapid** (left) and **patel2015conical** (right) showing the maximum lateral acceleration achieved with and without and active tail. Note the right graph manages similar results to the left graph.

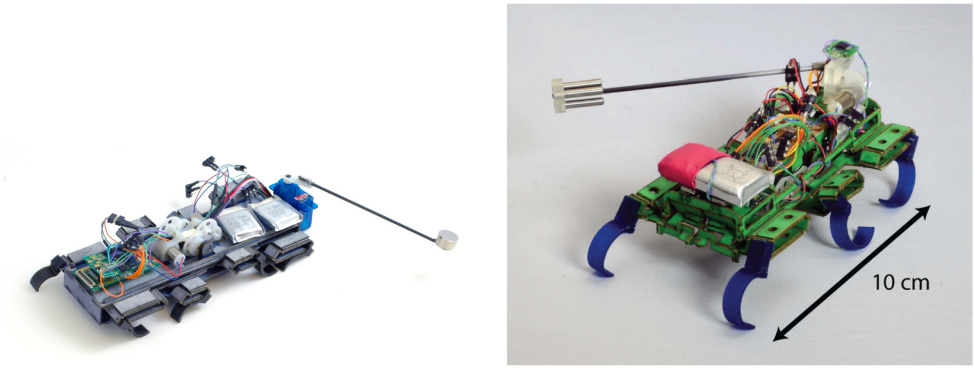

Figure 1.11: Images of the robots in **pullin2012dynamic** (left) and **kohut2013precise** (right).

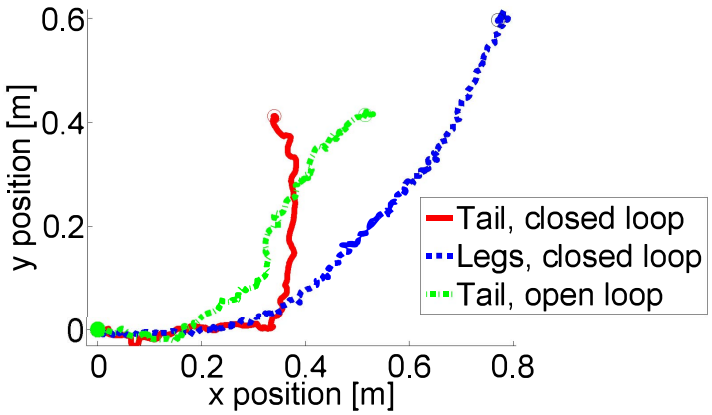

Figure 1.12: Data from **kohut2013precise** comparing the robot path on an XY plane for a $90°$ differential drive turn, open loop tail turn, and closed loop tail turn. Note the vastly increased sharpness of the turn when a tail is used.

1.3.6 *Terrestrial* → *Turning* → *Initiation*

pullin2012dynamic, **kohut2013precise** both use similar robot designs, insect like robots that locomote using 6-8 pairs of small legs (in this case **pullin2012dynamic** used a robot with eight legs, and **kohut2013precise** used six legs). Both robots are designed to be very light (52 g in **pullin2012dynamic** and 46 g in **kohut2013precise**) so the legs have a low friction force with the ground. A suitably weighted tail, when swung out in a horizontal motion, can overcome this friction force and impart enough torque to rotate the body of the robot to a new heading.

kohut2013precise compared a open and closed loop response of the tail, while **pullin2012dynamic** only compared open loop tail responses at different frequencies and amplitudes, as can be seen in figure **??**.

Both experiments were able to greatly increase the turning rate of the robot over a turn using a differential drive, at $360\,°\,s^{-1}$ for **kohut2013precise** and $400\,°\,s^{-1}$ for **pullin2012dynamic**.

1.3.7 *Terrestrial* → *Balancing* → *Stability*

The forces that may cause the robot to topple over when balancing can result from both *internal* forces: robot design or joint inertia when moving at high speed, and *external* forces:

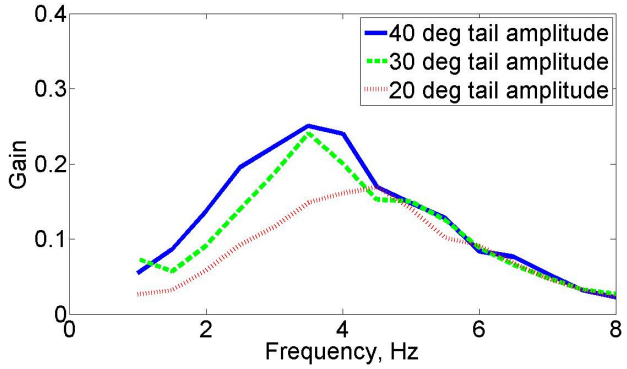

Figure 1.13: Data from **pullin2012dynamic** showing the gain in yaw rate for various open loop tail trajectories and different frequencies and amplitudes.

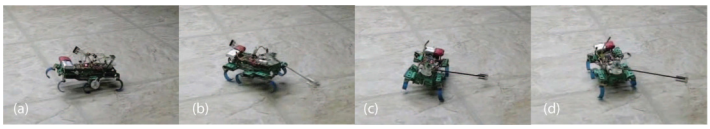

Figure 1.14: Images from **kohut2013precise** showing the robot using its tail to make a turn.

uneven terrain or impact. **takita2002development** is concerned with internal forces, whereas **briggs2012tails** is concerned with external forces.

takita2002development used a dinosaur like bipedal robot with a long neck and tail. The neck and tail then swung from side to side during the gait, maintaining the stability of the robot. Two experiments were conducted using different strategies for maintaining stability. The "static" method swung the neck and tail in a trapezoidal motion in order to keep the **COM!** (**COM!**) within the area of the current foot on the ground. The "dynamic" method calculated the **ZMP!** (**ZMP!**) of the robot and instead constrained that to keep it within the are of the foot. This resulted in a smaller motion of the neck and tail which enabled a faster gait.

briggs2012tails uses a quadrupedal robot closely modelled on a Cheetah which is hit in the torso by a "wrecking ball" to simulate a disturbance. In the control expermient the weighted tail remains static, in the active tail experiment the tail responds in an open loop trajectory

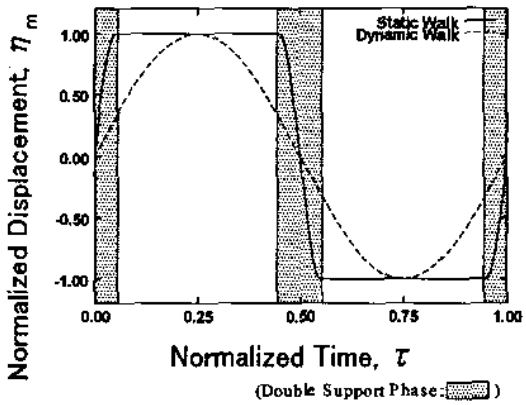

Figure 1.15: Data from **takita2002development** showing the normalised change in **COM!** for a static and dynamic walk.

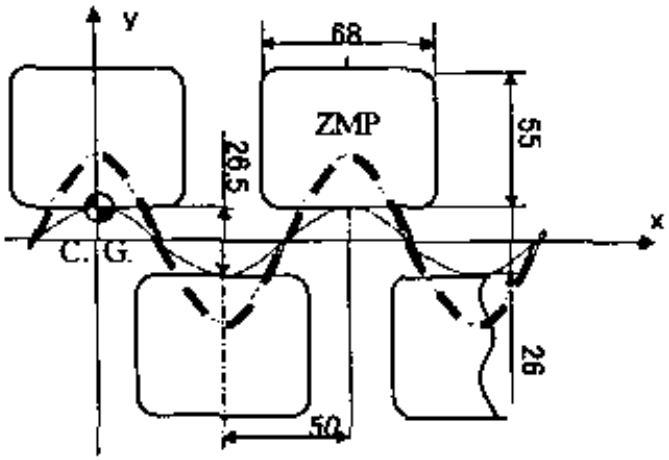

Figure 1.16: Data from **takita2002development** showing the trajectory of the **COM!** and **ZMP!** for a static and dynamic walk.

Figure 1.17: Video still of the TITRUS-III robot from **titrusvideo**.

when triggered by an accelerometer that sensed the impact. The active tail experiment was able to significantly reduce the hip displacement after impact, as can be seen in figure **??**.

1.3.8 *Transition → Hopping → Amplification*

1.3.9 *Aerial → Hopping → Stability*

1.3.10 *Aerial → Jumping → Initiation*

1.3.11 *Aerial → Jumping → Stability*

1.3.12 *Aerial → Falling → Stability*

1.4 Bio-Inspiration

1.5 Conclusion and Discussion

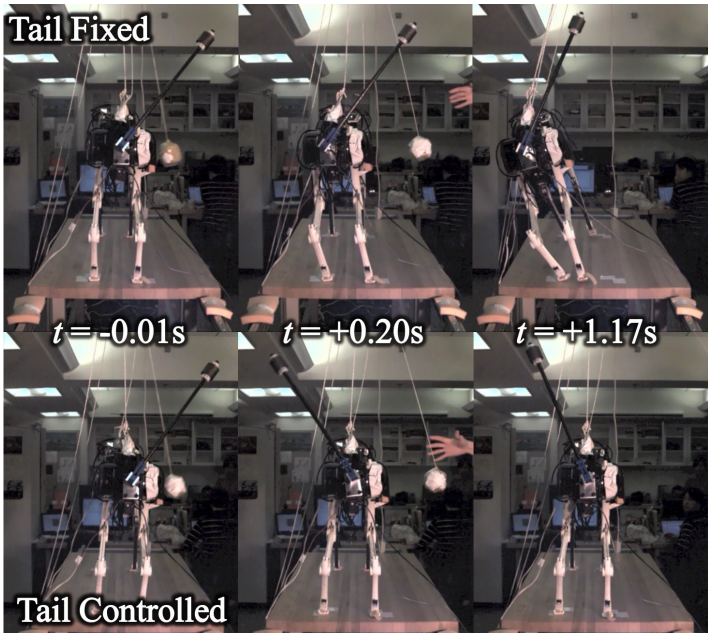

Figure 1.18: Imagers from **briggs2012tails** showing how the tail or body deflect when hit by the wrecking ball, depending on if the tail is active.

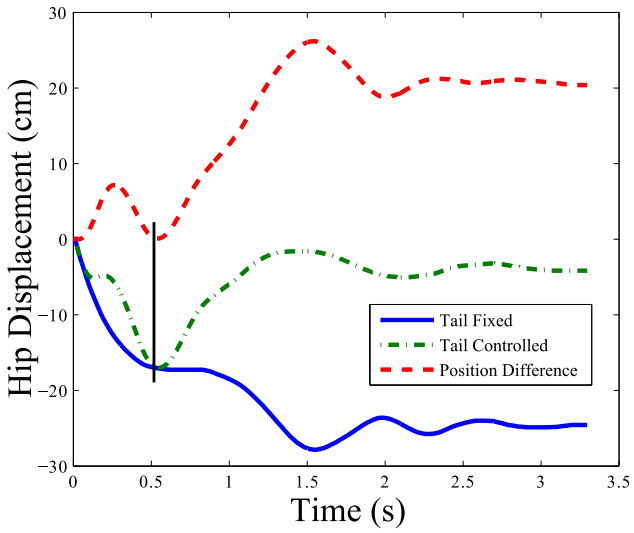

Figure 1.19: Data from **briggs2012tails** showing the difference in hip displacement between a fixed and controlled tail.

Chapter 2

Creating a Configurable Payload for Instability Experiments

2.1 Introduction

In order to generate a diverse set of test data for the experiments in chapter **??**, a configurable payload was conceived, an object that could be configured to have a wide range of masses and **COM!**. A series of test points can then be generated which have a specific mass and **COM!**, and a matching algorithm can be used to find the configuration that mostly closely matches these parameters. The experiments can then be run with each of these test points to generate the test data.

The payload consists of a matrix of cubes of various materials packed tightly into a **3D!** (**3D!**) printed container. The cubes are designed to be changed after each experimental run to alter the mass and **COM!** of the payload. A lid on the container prevents the cubes from falling out during the experiment, and the exterior design of the box may accommodate additional features to improving the handling of the payload by the robot arm.

The test points can then be generated by considering the *Configuration Space* of the payload design, i.e. how many permutations can be generated given a $n \times n \times n$ matrix of cubes, where each cube can be a number of different materials. The mass and **COM!** can then be calculated for each permutation, taking into taking into account the material density and mass and **COM!** of the container. "Extrema" test points can then be found simply by finding the permutation with the maximum or minimum mass and **COM!**, or combination thereof. Depending on the number of permutations, a search method can then be used that accepts an arbitrary mass and **COM!** as a target, and finds the nearest permutation to that target for other test point sets.

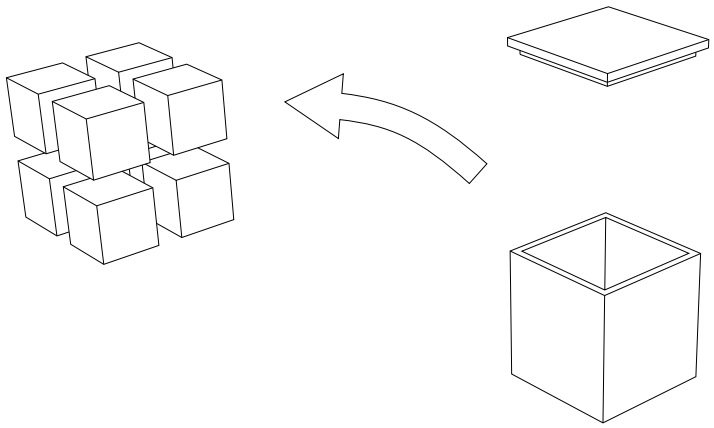

Figure 2.1: Concept drawing of the configurable payload.

2.2 Mathematical Design

2.2.1 Configuration Space

Firstly, consider a positive real set of material densities $\mathcal{P} \in \mathbb{R}^+$, each element the density (in $\mathrm{kg\,m^{-3}}$) of a material to be used:

$$\mathcal{P} = \{\rho_1, \rho_2 \dots \rho_n \mid \rho_i > 0\} \tag{2.1}$$

Each permutation can then be defined as an $n \times n \times n$ matrix $\boldsymbol{C}$, such that each element is an element of $\mathcal{P}$, where n^3 is the number of cubes in the matrix:

$$\boldsymbol{C} = (c_{ijk}) \in \mathbb{R}^{n^n} \mid (c_{ijk}) \in \mathcal{P} \tag{2.2}$$

$\mathcal{Z}$ can then be defined as the set of all permutations of $\boldsymbol{C}$.

To calculate the mass of the permutation, take the sum of all the cube densities multiplied by their volume a^3, where a is the cube edge length, plus the container mass m_c:

$$M\left(\boldsymbol{C}\right) = \left(\sum_{i=1}^{n}\sum_{j=1}^{n}\sum_{k=1}^{n} c_{ijk}a^3\right) + m_c \tag{2.3}$$

To calculate the **COM!**, take the sum of each cube mass multiplied by its position relative to the centroid of the center cube (c_{222}), which can be calculated from the cube indexes ijk, plus the container **COM!** $\boldsymbol{r}_c$ if non-zero:

$$R\left(\boldsymbol{C}\right) = \frac{\left(\sum_{i=1}^{n}\sum_{j=1}^{n}\sum_{k=1}^{n} c_{ijk}a^4\left(\begin{bmatrix} i & j & k \end{bmatrix} - n + 1\right)\right) + \boldsymbol{r}_c}{M\left(\boldsymbol{C}\right)} \tag{2.4}$$

The *configuration space* $\mathcal{Y}$ can then be considered as a set of $\mathbb{R}^4$ vectors containing the target mass and **COM!** concatenated as $\begin{bmatrix} m_i & \boldsymbol{r}_i \end{bmatrix}$ of each element. As such, $\mathcal{Y}$ is a codomain of $\mathcal{X}$, such that $H : \mathcal{X} \mapsto \mathcal{Y}$ where map function H is $\begin{bmatrix} M(\boldsymbol{C}) & R(\boldsymbol{C}) \end{bmatrix}$

2.2.2 Test Point Sets

Test points can either be derived from subsets of $\mathcal{X}$ defined by logical expressions, or the nearest neighbours of $\mathcal{Y}$ from a target mass and **COM!** concatenated into a vector as in H, found by a *search method* (see subsection **??**).

2.2.2.1 Extrema Set ($\mathcal{E}$)

The extrema set is designed to test the extremas of the space of $\mathcal{Z}$ for both $M(\mathcal{Z})$ and $R(\mathcal{Z})$. The extrema set if defined from a set of logical constraints. The first two constraints of the set find the maximum and minimum values of the payload mass using $M(\mathcal{Z})$, and the next four constraints use the payload **COM!** using $M(\mathcal{C})$ to get the maximum and minimum values of the x and y component of the **COM!**. Finally, the last four constraints define the diagonal maximum and minimum values where the **COM!** components match $x = y$ or $x = -y$.

$$\mathcal{E} = \left\{ \boldsymbol{x} \subset \mathcal{Z} \mid \begin{cases} M(\boldsymbol{x}) = \max\{M(\mathcal{Z})\} \\ M(\boldsymbol{x}) = \min\{M(\mathcal{Z})\} \\ R(\boldsymbol{x})_x = \max\{R(\mathcal{Z})_x\} \\ R(\boldsymbol{x})_x = \min\{R(\mathcal{Z})_x\} \\ R(\boldsymbol{x})_y = \max\{R(\mathcal{Z})_y\} \\ R(\boldsymbol{x})_y = \min\{R(\mathcal{Z})_y\} \\ R(\boldsymbol{x})_x = \max\{R(\mathcal{Z})_x\} \wedge R(\boldsymbol{x})_x = R(\boldsymbol{x})_y \\ R(\boldsymbol{x})_x = \min\{R(\mathcal{Z})_x\} \wedge R(\boldsymbol{x})_x = R(\boldsymbol{x})_y \\ R(\boldsymbol{x})_x = \max\{R(\mathcal{Z})_x\} \wedge R(\boldsymbol{x})_x = -R(\boldsymbol{x})_y \\ R(\boldsymbol{x})_x = \min\{R(\mathcal{Z})_x\} \wedge R(\boldsymbol{x})_x = -R(\boldsymbol{x})_y \end{cases} \right\} \tag{2.5}$$

Mass Limited $\mathcal{E}$ When this set was generated, it was found that $M(\mathcal{E}_1)$ was greater than the chosen robot arm could safely lift. Therefore, $M(\boldsymbol{x}) = \max\{M(\mathcal{Z})\}$ in $\mathcal{E}$ was changed to $\begin{bmatrix} m_{max} & 0 & 0 & 0 \end{bmatrix}$ where m_{max} is the safe mass limit that the robot arm can lift. One of the search methods described in section **??** can then be used to find the nearest point in configuration space.

2.2.2.2 Cube Set ($\mathcal{C}$)

The cube set is defined by the vertices of a cube of size b centred around the **COM!** origin $\begin{bmatrix}0 & 0 & 0\end{bmatrix}$.

$$\mathcal{C} = \left\{ \boldsymbol{x} \subset \mathcal{C} \mid \begin{bmatrix}\pm\frac{b}{2} & \pm\frac{b}{2} & \pm\frac{b}{2}\end{bmatrix} = \boldsymbol{x} \right\} \tag{2.6}$$

2.2.2.3 Balanced Set ($\mathcal{B}$)

The balanced set is defined by q points in $\mathcal{C}$ subject to the constraint $R(\boldsymbol{x})_x = 0 \wedge R(\boldsymbol{x})_y = 0$. This can be defined as a "balanced" set as the **COM!** x and y components are both zero. The points are evenly spaced between the maximum and minimum mass as defined in section **??**.

$$\begin{aligned} m_r &= \frac{\max\{M(\mathcal{Z})\} - \min\{M(\mathcal{Z})\}}{q+1} \\ \boldsymbol{z} &= \begin{bmatrix} m_r & 2m_r & \cdots & qm_r \end{bmatrix} \\ \mathcal{B} &= \{\boldsymbol{x} \subset \mathcal{C} \mid z_i = \boldsymbol{x} \wedge R(\boldsymbol{x})_x = 0 \wedge R(\boldsymbol{x})_y = 0\} \end{aligned} \tag{2.7}$$

2.2.3 Search Methods

When considering a viable search method given a target, the cardinality of $\mathcal{X}$ is important to consider. It is defined as $|\mathcal{X}| = |\mathcal{P}|^{n^3}$ which increases super exponentially with n. For example, when $|\mathcal{P}| = 4$, $n = 2$ results in 65536 permutations and $n = 3$ results in approximately 1.8×10^{16} permutations. It's very clear that when $n > 2$ for non-trivial cardinalities of $\mathcal{P}$, any kind of brute-force method is not computationally tractable. Therefore, a brute-force nearest neighbour method (see subsection **??**) would be suitable for when $n = 2$, and a heuristic search method such as simulated annealing (see subsection **??**) method would be suitable for when $n > 2$.

2.2.3.1 Multiobjective Simulated Annealing

Simulated annealing **kirkpatrick1983optimization** is a modification to a gradient descent optimisation that allows the algorithm the chance to "jump out" of local minima early on (even though the approximation becomes temporarily worse). However, as the number of remaining steps decreases, that probability becomes smaller, becoming more and more like gradient descent. First, like any gradient descent algorithm, two things need to be generated, the initial configuration $\boldsymbol{C_0}$, which can be random or manually selected, and the function $\mathcal{N}(\boldsymbol{C})$ which creates a set of all the "neighbours" of $\boldsymbol{C}$. In this case, this can be defined as the subset of $\mathcal{X}$ where the difference between $\boldsymbol{C}$ and an element of $\mathcal{N}(\boldsymbol{C})$ is one and only one $c_{ijk} \neq c_{ijk}$:

$$\mathcal{N}(\boldsymbol{C}) = \{x \subset \mathcal{X} \mid \exists! \, (x_{ijk} \neq c_{ijk})\} \tag{2.8}$$

Then the simulated annealing function can be described as follows:

1. Set $\boldsymbol{C}$ to the initial permutation $\boldsymbol{C_0}$.
2. For each of the optimisation steps:
   (a) Set the temperature value t with function $T\left(\frac{k_{max}}{k}\right)$ which takes into account the number of remaining steps.
   (b) Set $\boldsymbol{C}_{new}$ as a random element from the set of all neighbours of $\boldsymbol{C}$ as defined by $\mathcal{N}(\boldsymbol{C})$.
   (c) Use acceptance probability function $P\left(E\left(\boldsymbol{C}\right), E\left(\boldsymbol{C}_{new}\right), t\right)$ where $E\left(\boldsymbol{C}\right)$ is the energy function.
   (d) Compare that value with a random uniformly distributed real number between 0 and 1. If greater than or equal to, then replace $\boldsymbol{C}$ with $\boldsymbol{C}_{new}$. Otherwise, keep it the same.
   (e) Repeat with $\boldsymbol{C}$ until there are no remaining steps.
3. Return the approximated permutation $\boldsymbol{C}$.

$\boldsymbol{C} = \boldsymbol{C}_0$
for $k \leftarrow 1, k_{max}$ **do**
  $t = T\left(\frac{k_{max}}{k}\right)$
  $\boldsymbol{C}_{new} = \mathcal{N}(\boldsymbol{C}) \xleftarrow{R} x$
  if $P\left(E\left(\boldsymbol{C}\right), E\left(\boldsymbol{C}_{new}\right), t\right) \geq x \sim U\left([0,1]\right)$ **then**
    $\boldsymbol{C} = \boldsymbol{C}_{new}$
  end if
end for
return $\boldsymbol{C}$

Energy Function Simulated annealing can also be adapted for multi-objective optimisation **serafini1994simulated**, so it is possible to generate test points that approximate a desired mass and **COM!** simultaneously.

Cooling Function The function which controls the probability of exiting local minima (known as the *temperature*) is known as the *cooling function*. This function can be any function which monotonically decreases (except in adaptive simulated annealing where it is dependant on the accuracy of the current approximation). Different functions will result in a different cooling profile, generally decreasing quickly in the first few steps, and then slowing down after that.

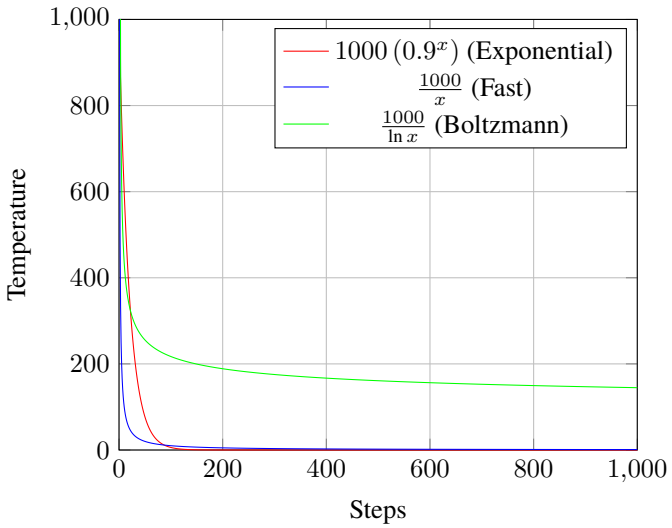

Figure 2.2: Various temperature cooling profiles for simulated annealing, assuming 1000 steps.

2.2.3.2 Nearest Neighbour

If $\mathcal{X}$ is suitably small, then a brute-force method can be used which is guaranteed to find the nearest element to the target within a finite time. This can be done by calculating the L2 norms between the target vector t and all the elements of $\mathcal{Y}$ and finding the minimum. If there are several elements in the domain of $\mathcal{X}$, then one is chosen at random from this set.

$$NN\left(t, \mathcal{X}\right) = \min\left\{\left\|t - x\right\|_2 \mid \forall x \in \mathcal{Z}\right\} \tag{2.9}$$

2.3 Implementation

2.3.1 Container Design

The internal width of the container was chosen to be 75 mm, which combined with a wall width of 5 mm gives an overall width of 1 mm. Therefore, each cube would be $\frac{75}{n}$mm in size.

2.3.2 Selected Search Method

Initially an $n = 3$ configuration was used with the acceptance probability function *Rule M* from **serafini1994simulated**. This is a weighted blend of two other algorithms defined in the paper, *Rule P* and *Rule W* with a weighting coefficient $\alpha \in (0, 1) \subset \mathbb{R}$. There is also a weighting vector for each element of the test point $\boldsymbol{w} \in \mathbb{R}^4 \mid w_i \in (0, 1)$.

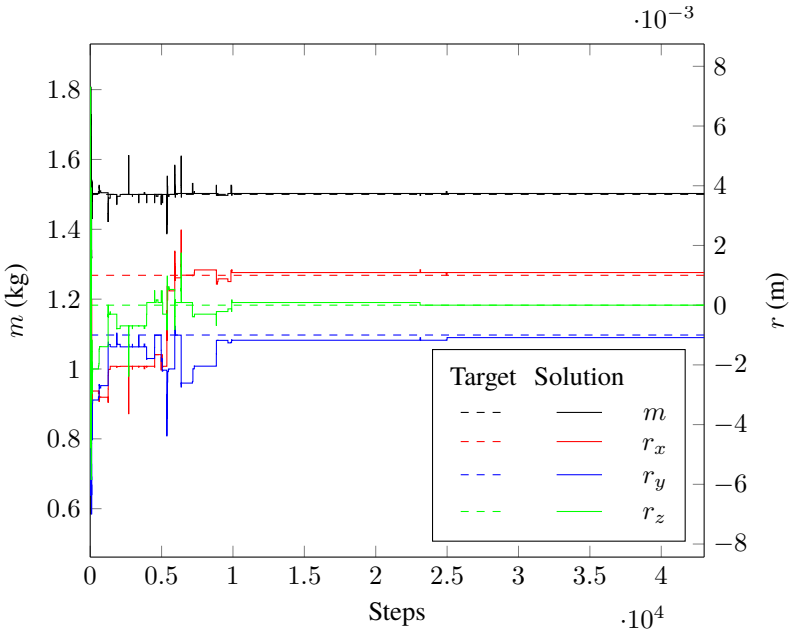

Figure 2.3: Simulated annealing output for the target $[1.5 \quad 0.001 \quad 0.001 \quad 0.001]$ with $\alpha = 0.997$ and even weighting $w_m, \boldsymbol{w_r} = 0.25$ for 4.3×10^4 steps.

$$P\left(\boldsymbol{x}, \boldsymbol{y}, \boldsymbol{w}, t\right) = \alpha \underbrace{\prod_{i=1}^{m} \min\left\{1, e^{\frac{w_i(x_i - y_i)}{t}}\right\}}_{\text{Rule P}} + (1-\alpha) \underbrace{\min\left\{1, \max_{i=1,\ldots,m}\left\{1, e^{\frac{w_i(x_i - y_i)}{t}}\right\}\right\}}_{\text{Rule W}} \tag{2.10}$$

Unfortunately it was difficult to find a stable and consistent result even after a long time running the algorithm.

Therefore as an alternative, the $n = 2$ configuration was used, with larger cubes to compensate.

2.3.3 Material Selection

In order to produce a reasonably wide and dense configuration space, four materials: *wood*, *plastic*, *aluminium* and *steel*, were chosen. More dense materials, such as nickel and lead, were rejected due to difficulty sourcing stock of the correct size, or issues with machining. Initially estimated densities were used in order to test the simulated annealing algorithm, but after the cubes were manufactured, it was possible to get an average density based on the measured mass of each cube as seen in figure **??**, given a cube size of 35 mm. Table **??** lists the exact kind of material used, and its calculated density. These differ from many stated values available from other sources such as online material databases, likely de to small discrepancies in cube size due to manufacturing tolerances and variability in material composition (particularly for wood since the blocks required sanding in order to fit in the container, and due to the less precise properties of natural materials).

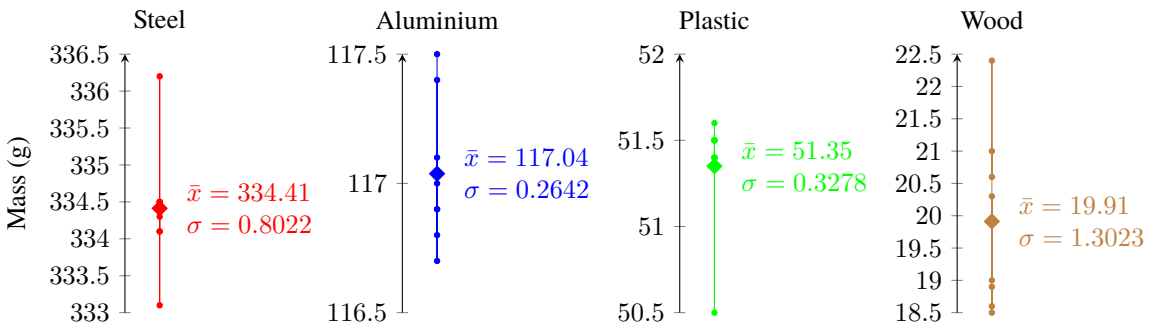

Figure 2.4: Masses for each set of eight 35 mm cubes of the configurable payload for each of the four materials, with the mean mass $\bar{x}$ and standard deviation σ of each set.

Material	Variant	Density (kg m^{-3})
Wood	Pine	464.37
Plastic	Acrylic	1201.9
Aluminium	6082	2740
Steel	EN3B	7800

Table 2.1: The materials chosen for the cubes.

2.4 Results

2.4.1 Configuration Space

Given a $2 \times 2 \times 2$ matrix of cubes with the materials in table **??**, there were a total of 65536 permutations, with a total mass range of $0.38027891, 2.8964000000000003$kg, $and a total$**COM!**$rang$

$$-0.013438032924318489, 0.013438032924318487$$

mm$on all axes. A some permutations mapped to the same point in con figuration space, there were 6$
$(\textbf{com!})vectors.$

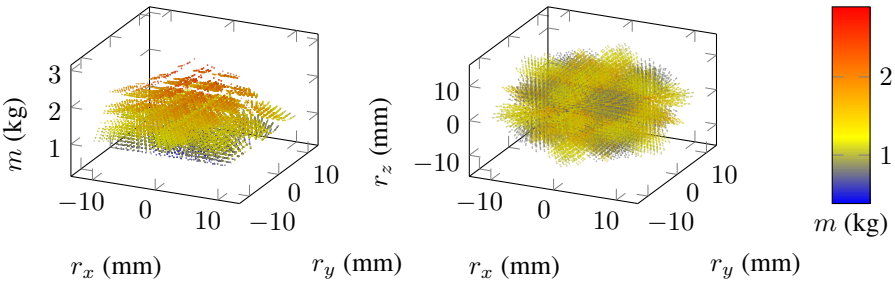

Figure 2.5

m	$\boldsymbol{r}$
Extrema Set ($\mathcal{E}$)	
1.204	$\begin{bmatrix}0.012 & 0.000 & 0.000\end{bmatrix}$
1.204	$\begin{bmatrix}0.000 & 0.012 & 0.000\end{bmatrix}$
1.204	$\begin{bmatrix}-0.012 & -0.000 & 0.000\end{bmatrix}$
1.204	$\begin{bmatrix}0.000 & -0.012 & 0.000\end{bmatrix}$
0.380	$\begin{bmatrix}0.000 & 0.000 & 0.000\end{bmatrix}$
1.009	$\begin{bmatrix}0.011 & 0.011 & 0.000\end{bmatrix}$
1.009	$\begin{bmatrix}-0.011 & -0.011 & 0.000\end{bmatrix}$
1.009	$\begin{bmatrix}0.011 & -0.011 & 0.000\end{bmatrix}$
1.009	$\begin{bmatrix}-0.011 & 0.011 & 0.000\end{bmatrix}$

Table 2.2: Table of the vectors of $\mathcal{E}$, excluding the mass-limited element.

Target		Nearest		L2 Norm Error
m	$\boldsymbol{r}$	m	$\boldsymbol{r}$	
Extrema Set ($\mathcal{E}$)				
1.250	$\begin{bmatrix}0.000 & 0.000 & *\end{bmatrix}$	1.204	$\begin{bmatrix}0.000 & 0.000 & -0.009\end{bmatrix}$	4.556×10^{-2}
Cube Set ($\mathcal{C}$)				
$*$	$\begin{bmatrix}-0.007 & -0.007 & -0.007\end{bmatrix}$	0.987	$\begin{bmatrix}-0.007 & -0.007 & -0.007\end{bmatrix}$	5.244×10^{-4}
$*$	$\begin{bmatrix}-0.007 & -0.007 & 0.007\end{bmatrix}$	0.987	$\begin{bmatrix}-0.007 & 0.007 & -0.007\end{bmatrix}$	2.023×10^{-2}
$*$	$\begin{bmatrix}-0.007 & 0.007 & -0.007\end{bmatrix}$	0.987	$\begin{bmatrix}0.007 & -0.007 & -0.007\end{bmatrix}$	2.023×10^{-2}
$*$	$\begin{bmatrix}-0.007 & 0.007 & 0.007\end{bmatrix}$	0.987	$\begin{bmatrix}0.007 & 0.007 & -0.007\end{bmatrix}$	2.023×10^{-2}
$*$	$\begin{bmatrix}0.007 & -0.007 & -0.007\end{bmatrix}$	0.987	$\begin{bmatrix}-0.007 & -0.007 & 0.007\end{bmatrix}$	2.023×10^{-2}
$*$	$\begin{bmatrix}0.007 & -0.007 & 0.007\end{bmatrix}$	0.987	$\begin{bmatrix}-0.007 & 0.007 & 0.007\end{bmatrix}$	2.023×10^{-2}
$*$	$\begin{bmatrix}0.007 & 0.007 & -0.007\end{bmatrix}$	0.987	$\begin{bmatrix}0.007 & -0.007 & 0.007\end{bmatrix}$	2.023×10^{-2}
$*$	$\begin{bmatrix}0.007 & 0.007 & 0.007\end{bmatrix}$	0.987	$\begin{bmatrix}0.007 & 0.007 & 0.007\end{bmatrix}$	5.244×10^{-4}
Balanced Set ($\mathcal{B}$)				
0.380	$\begin{bmatrix}0.000 & 0.000 & *\end{bmatrix}$	0.771	$\begin{bmatrix}-0.000 & -0.000 & -0.004\end{bmatrix}$	3.903×10^{-1}
1.190	$\begin{bmatrix}0.000 & 0.000 & *\end{bmatrix}$	1.136	$\begin{bmatrix}-0.000 & -0.000 & 0.001\end{bmatrix}$	5.434×10^{-2}
2.000	$\begin{bmatrix}0.000 & 0.000 & *\end{bmatrix}$	1.204	$\begin{bmatrix}0.000 & 0.000 & -0.009\end{bmatrix}$	7.956×10^{-1}

Table 2.3: Table of the target and actual vectors for $\mathcal{C}$, $\mathcal{B}$ and the mass limited element of $\mathcal{E}$ with the L2 norm error. $*$ notation indicates "don't care" and is excluded from the search algorithm.

2.4.2 Test Points

2.4.2.1 Mass and COM!

2.4.2.2 Material Permutations

2.5 Discussion and Conclusion

2.5.1 Discussion

- Talk about the limitations on **COM!**, ± 10 mm is pretty small, but expect to see some differences in data (spoiler alert - it mostly didn't).
- Talk about mass limitation due to robot arm but also expect to see differences (this time it did!).

m	$\boldsymbol{r}$	Material Matrix	3D Preview
		Extrema Set ($\mathcal{E}$)	
1.204	$[0.000 \quad 0.000 \quad -0.009]$	S W A S W A W W	
1.204	$[0.012 \quad 0.000 \quad 0.000]$	W S W A W A W S	
1.204	$[0.000 \quad 0.012 \quad 0.000]$	W W S A W W A S	
1.204	$[-0.012 \quad -0.000 \quad 0.000]$	A W S W S W A W	
1.204	$[0.000 \quad -0.012 \quad 0.000]$	A S W W S A W W	
0.380	$[0.000 \quad 0.000 \quad 0.000]$	W W W W W W W W	
1.009	$[0.011 \quad 0.011 \quad 0.000]$	W W W S W W W S	
1.009	$[-0.011 \quad -0.011 \quad 0.000]$	S W W W S W W W	
1.009	$[0.011 \quad -0.011 \quad 0.000]$	W S W W W S W W	
1.009	$[-0.011 \quad 0.011 \quad 0.000]$	W W S W W W S W	

Table 2.4

- Future plans for partially fluid filled box with range of density and viscosity to test liquid payloads?
- Anything else?

m	$\boldsymbol{r}$	Material Matrix	3D Preview
Cube Set ($\mathcal{C}$)			
0.987	$[-0.007 \quad -0.007 \quad -0.007]$	S A A W A W W W	
0.987	$[-0.007 \quad 0.007 \quad -0.007]$	A W S A W W A W	
0.987	$[0.007 \quad -0.007 \quad -0.007]$	A S W A W A W W	
0.987	$[0.007 \quad 0.007 \quad -0.007]$	W A A S W W W A	
0.987	$[-0.007 \quad -0.007 \quad 0.007]$	A W W W S A A W	
0.987	$[-0.007 \quad 0.007 \quad 0.007]$	W W A W A W S A	
0.987	$[0.007 \quad -0.007 \quad 0.007]$	W A W W A S W A	
0.987	$[0.007 \quad 0.007 \quad 0.007]$	W W W A W A A S	

Table 2.5

2.5.2 Conclusion

This work has outlined the design and implementation of a configurable payload that is suitable for the experiments in chapter **??**. Using this payload, a range of objects with different mass and **COM!** can be emulated in order to generate a wide range of experimental data.

m	$\boldsymbol{r}$	Material Matrix	3D Preview
Balanced Set ($\mathcal{B}$)			
0.771	$[-0.000 \quad -0.000 \quad -0.004]$	A A W A W W A W	
1.136	$[-0.000 \quad -0.000 \quad 0.001]$	P W W S S P P P	
1.204	$[0.000 \quad 0.000 \quad -0.009]$	S W A S W A W W	

Table 2.6

??

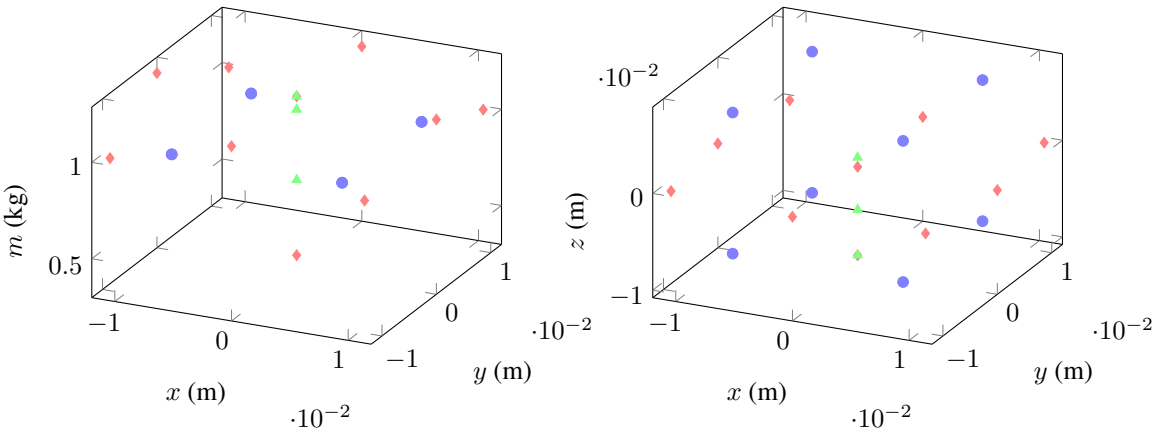

Figure 2.6: Mass and **COM!** coordinates for each test point set.

Chapter 3

Investigating the use of a 2DOF Pendulum Tail for Compensating for Instability when Carrying a Payload

3.1 Introduction

3.2 Control Experiments

3.2.1 Results

3.3 Conclusion and Discussion

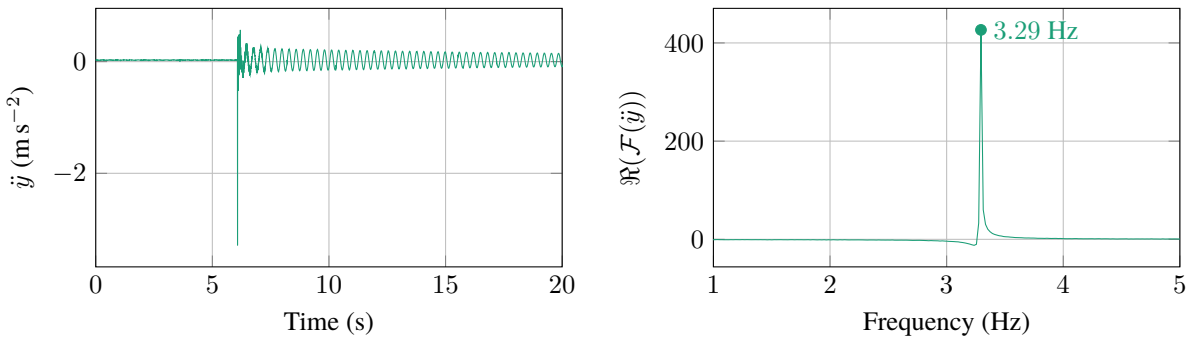

Figure 3.1: Resonant frequency of the tail calculated from accelerometer data captured during an impact with a steel hammer. The left graph is the accelerometer data, and the right graph is the real part from a real **DFT!** (**DFT!**) on the data.

??

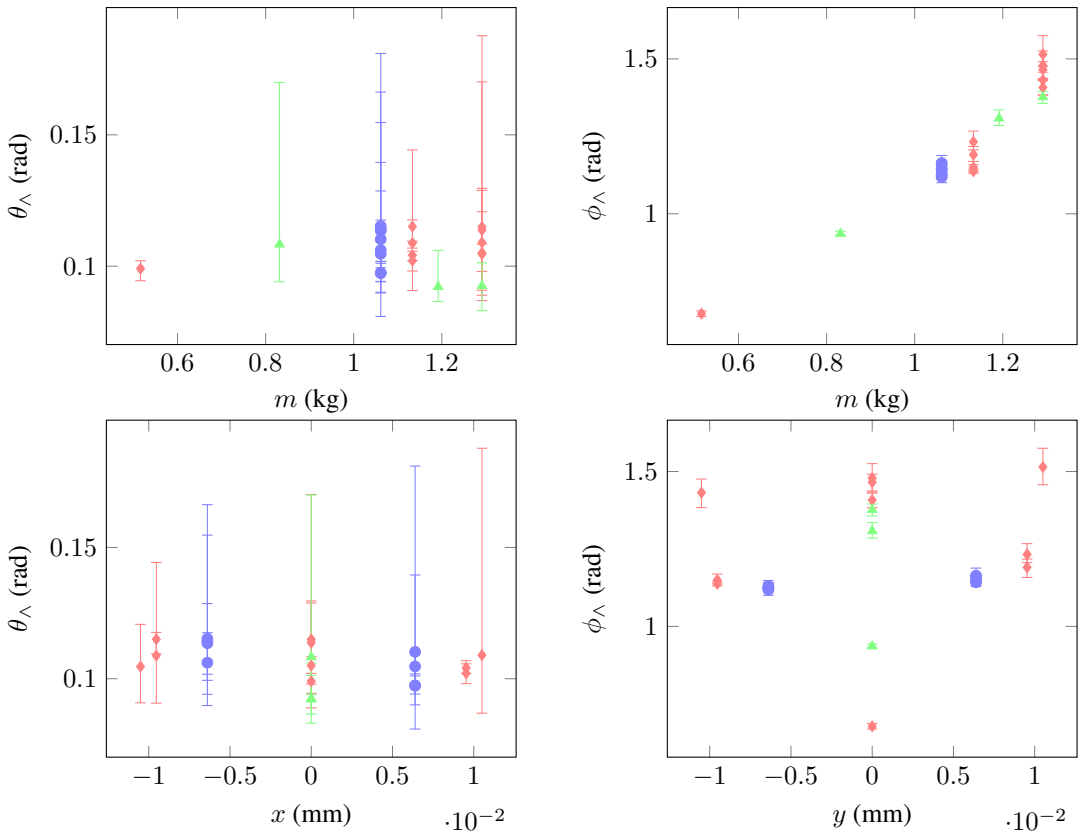
$\theta_\wedge$ (rad)
0.15
0.1
0.6
0.8
1
1.2
m (kg)
$\phi_\wedge$ (rad)
1.5
1
0.6
0.8
1
1.2
m (kg)
$\theta_\wedge$ (rad)
0.15
0.1
−1
−0.5
0
0.5
1
x (mm)
$\cdot 10^{-2}$
$\phi_\wedge$ (rad)
1.5
1
−1
−0.5
0
0.5
1
y (mm)
$\cdot 10^{-2}$

Figure 3.2

Appendices